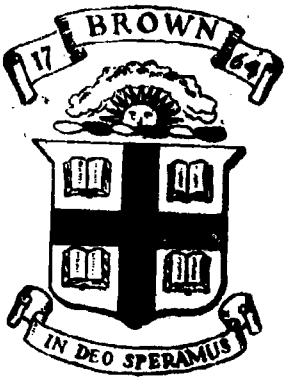

Division of Engineering
BROWN UNIVERSITY
PROVIDENCE, R. I.

AN EXPERIMENTAL METHOD FOR MEASURING THE ELECTRICAL CONDUCTIVITY OF HIGH TEMPERATURE GASES

BY

G. F. ANDERSON

United States Air Force
Air Force Office of Scientific Research
Grant No. AF-AFOSR-62-111
Technical Report WT-35

June 1962

AN EXPERIMENTAL METHOD FOR MEASURING THE ELECTRICAL CONDUCTIVITY OF HIGH TEMPERATURE GASES

by

Gordon F. Anderson

Technical Report WT-35

DIVISION OF ENGINEERING

BROWN UNIVERSITY

PROVIDENCE, RHODE ISLAND

June 1962

Sponsored by:

United States Air Force

Air Force Office of Scientific Research

Grant No. AF-AFOSR-62-111

PREFACE

The preliminary work on this project, the construction of facility and the purchase of most of the instrumentation was supported by the Division of Engineering, Brown University. From October 1961, the work has been supported by the United States Air Force, Office of Scientific Research Grant AF-AFOSR-62-111.

The work on this project was submitted by the author as a Thesis in partial fulfillment of the requirements for the Degree of Doctor of Philosophy in the Division of Engineering, Brown University, June 1962.

Credit is due Dr. Paul F. Maeder for his assistance in all phases of this investigation.

ABSTRACT

The feasibility of utilizing the effect of a conducting medium on the impedance of a small coil for the measurement of the conductivity of high temperature gases is first investigated theoretically and then developed experimentally.

The method described in this report is particularly well suited for measuring the electrical conductivity of gases at high densities.

Data which have been obtained for air in the range of 5 mhos/meter to 250 mhos/meter at atmospheric density are included in the report to illustrate the use and feasibility of the experimental technique.

LIST OF SYMBOLS

A	Constant Defined on Page 5, $\frac{8}{3}\sqrt{\frac{2k}{\pi me}}$
D	Debye Shielding Length, $\sqrt{\frac{kT}{4\pi e^2 n_e}}$
E	Electric Field Strength
H	Magnetic Field Strength
$H_n^{(2)}$	Hankle Function of Second Kind, Order n (Jahnke and Emde)
I	Electric Current
J_n	Bessel Function of First Kind, Order n (Jahnke and Emde)
K	Correction Coefficient Defined on Page 3
Q	Collision Cross Section
R	Radius of Coil
R	Electric Resistance
R_M	Magnetic Reynolds Number
T	Temperature
U_∞	Free Stream Velocity in x - Direction
V	Induced Voltage
a	Diameter of Neutral Particle for Elastic Collisions
e	Electric Charge on Electron
$\vec{e}$	Unit Vector
i	Imaginary Quantity, $i = e^{i\frac{\pi}{2}} = \sqrt{-1}$
j	Electric Current Density
k	Boltzmann Constant
l	Length of Coil
m	Mass of Gas Particle

LIST OF SYMBOLS (continued)

n	Number Density
n	Number of Turns in a Coil
p	Variable in Fourier Transform
u	Dimensionless Parameter Equal to $\beta R_M^{1/2}$
v	Electron Velocity
v	Dimensionless Parameter Equal to $p R_M^{1/2}$
Φ	Magnetic Flux
ψ	Dependent Variable Defined by $\varphi = r\psi$
β	Dimensionless Parameter Equal to $\sqrt{-[(\lambda^2 p^2 + \frac{R_M''}{R_M}) + i(1 - p\lambda \frac{R_M'}{R_M^{1/2}})]}$
ε	Dielectric Constant
λ	Ratio of Coil Radius to Coil Length
μ	Permeability
μ_o	Permeability of Free Space
ν	Collision Frequency
ξ	Dimensionless Variable, $\frac{x}{l} R_M^{1/2}$
ρ	Dimensionless Variable, $\frac{r}{R} R_M^{1/2}$
σ	Electrical Conductivity
φ	Magnetic Flux Amplitude
ω	Electric Field Frequency
ω_p	Plasma Frequency

LIST OF SYMBOLS (continued)

Subscripts

e	Electrons
i	Ions
j	jth Species
m	Neutral Particles
r	Pertaining to the r - Direction
r	Partial Differential with Respect to r
x	Pertaining to the x - Direction
x	Partial Differential with Respect to x
ξ	Partial Differential with Respect to ξ
ρ	Partial Differential with Respect to ρ
+	Boundary Condition taken at (R + 0)
-	Boundary Condition taken at (R - 0)

Other

$(\overline{\ })$	Average Value
$(\vec{\ })$	Vector Quantity
$1[\ ]$	Unit Step Function

TABLE OF CONTENTS

TABLE OF CONTENTS (continued)

Page

LIST OF FIGURES

INTRODUCTION

Theoretical studies of the electrical properties of thermally ionized gases have been reported by a number of investigators. The electrical conductivity is derived by considering the motion of the electrons under the influence of an electrical field and collisions with the various components of the gas. The collision frequency is determined by statistical methods. Currents due to the motion of ions are neglected.

If the strength of the applied electric field varies with time, the currents in the plasma are due to both conduction and polarization. If, however, the frequency (ω) of an alternating applied electric field is small compared to the average electron collision frequency ($\bar{\nu}$), the polarization currents vanish. Only the electric properties with this condition imposed ($\omega << \bar{\nu}$), are of interest in this report.

The conductivity is found to be proportional to $n_e e^2/m_e \bar{\nu}$ where n_e is the number density of the electrons, e is the electric charge on the electron, and m_e is the mass of the electron.

There is disagreement among the authors reviewed on the averaging procedure to be employed for determining $\bar{\nu}$, and for this reason, quantitative agreement is not obtained in all the available theoretical literature. The disagreement is of the order of the differences between the most probable velocity, the average velocity and the root mean square velocity calculated for a Maxwellian velocity distribution.

In the following, the methods and results of Ref. (1) are reviewed to show the basis of the theoretical values used in this report.

The first approximation to the collision frequencies, which is derived from the Boltzmann kinetic equation for a Maxwellian velocity distribution, is given by:

$$\bar{\nu}_j = \frac{\sqrt{2}}{3\pi}\left(\frac{m_e}{kT}\right)^{5/2}\int_0^\infty \nu_j(v) v^4 e^{-\frac{m_e v^2}{2kT}} dv \tag{1}$$

For elastic collisions between electrons and uncharged particles:

$$\nu_{m_j}(v) = \pi a_j^2 N_{m_j} v \tag{2}$$

For collisions between electrons and ions,

$$\nu_i(v) = 2\pi n_i \frac{e^4}{m_e^2 v^3} \ln\left(\frac{D^2 m_e^2 v^4}{e^4}\right) \tag{3}$$

where D is the Debye shielding length which is defined as the distance at which the effect of the Coulomb field of a particular charged particle is shielded by the other distributed charged particles, and which has the value $\sqrt{\frac{kT}{4\pi e^2 n_e}}$. The impact length is defined as the distance of closest approach between an electron and ion for the electron to be defected 90° and has the value $e^2/m_e v^2$.

Substituting equation (2) into equation (1) yields the average collision frequency for collisions between electrons and neutral particles.

$$\bar{\nu}_{m_j} = \frac{8\sqrt{2}}{3\sqrt{\pi}}\sqrt{\frac{kT}{m_e}}\,\pi a_j^2 n_{m_j} \tag{4}$$

By substituting equation (3) into equation (1), the average electron collision frequency for collisions between electrons and ions is obtained.

$$\bar{\nu}_i = \frac{2}{3}\sqrt{8\pi}\,\frac{e^4 n_i}{\sqrt{m_e}(kT)^{3/2}} \ln \frac{kTD}{e^2} \tag{5}$$

The conductivity with the condition $(\omega << \bar{\nu})$ imposed is then given by:

$$\sigma = \frac{n_e e^2}{m_e(\Sigma \bar{\nu}_{m_j} + \bar{\nu}_i)} \tag{6}$$

Extending the analysis to a higher order of approximation, which in effect accounts for the effect of collisions on the electron velocity distribution, it is found that the conductivity may be expressed by:

$$\sigma = \frac{n_e e^2}{m_e(\Sigma \bar{\nu}_{m_j} + \bar{\nu}_i)} K_\sigma \tag{7}$$

where K_σ is a function of ω and the type of collisions taking place.

As reported in Ref. (1), for $(\omega >> \bar{\nu})$ where collisions play a small role in determining the motion of the electrons, K_σ is equal to unity. (The approximate Equ. (7) is, however, not valid in this case.) For $(\omega << \bar{\nu})$, however, which is the case of interest here, K_σ has the value 1.13 for electron collisions with neutral particles, and has the value 3.39 for collisions involving electrons and ions. If the interelectron collisions are considered as well as the electron-ion collisions, K_σ has the value 1.95.

The elementary analysis which leads to Equ. (6) is based on a Maxwellian electron velocity distribution, and K_σ may be considered as a correction to the elementary analysis which accounts for the effect of collisions on the electron velocity distribution.

Using this latter theoretical result as a basis for comparison, it was thought that experimental results over a large range of densities and temperatures would be of interest. Previous experimental works have usually been concerned with simulating upper atmospheric conditions and therefore were limited to relatively low densities.

In addition to the academic interest in the properties of materials under all conditions, the present interest in the field of magnetohydrodynamic power generation provides a definite need for information on the conductivity of high density gases.

The development of an experimental technique for measuring the conductivity of gases at higher densities than had previously been measured was the major purpose of this project.

The techniques described in Ref. (2) and Ref. (3) use the gas in the region behind the initial shock wave in a shock tube as the test gas. Extending the range of measurements to higher densities would require extreme shock tube driver pressures. Furthermore, since the coils used in both methods are external to the shock tube, a pyrex tube section is required at the measuring station and thus the allowable tube pressure is severely limited.

The shock wave reflected from the end plate of a shock tube would produce the desired experimental conditions, and it therefore was required to devise a method for measuring the conductivity of the gas contained in this region of the shock tube.

The method of Ref. (2) could not be adapted to measurements behind the shock reflected from the end of the shock tube because the measurements require that the test gas be in motion.

The method of Ref. (3) could be adapted to the stagnant region behind the reflected shock, and if the measuring coil were placed inside the shock tube, this method would be identical to the method described in this paper except for the technique employed in the electronic instrumentation.

The techniques for measuring conductivity in both Ref. (3) and this report are based on measuring the effect of a conducting medium on the impedance of a coil.

In the method of Ref. (3), the change in impedance of the coil alters the frequency of an oscillator and is detected by standard frequency modulation equipment.

In the investigation to be reported, the change in coil impedance is measured similar to an unbalance in an alternating current bridge circuit, although an actual bridge circuit is not employed.

Preliminary measurements of the conductivity of air at atmospheric density from 5 mhos per meter to 250 mhos per meter are included to illustrate the use and the feasibility of this new technique.

I. Theoretical Considerations

A - Conductivity

In order to determine the more important characteristics of the variation of the electrical conductivity with temperature and density, it is assumed that the collision cross sections for elastic collisions between the neutral particles and electrons have a weak dependence on temperature, Ref. (2), and in addition, an average cross section is assumed for all neutral particles. Equation (4) may then be written

$$\bar{\nu}_m = n_m \bar{Q}_m A T^{1/2} \tag{8}$$

where $A = \frac{8}{3}\sqrt{\frac{2k}{\pi m_e}}$. The conductivity according to Equ. (7) then becomes:

$$\sigma = \frac{n_e e^2}{m_e(\bar{\nu}_m + \bar{\nu}_i)} \left[\frac{\bar{\nu}_m}{(\bar{\nu}_m + \bar{\nu}_i)} K_{\sigma_m} + \frac{\bar{\nu}_i}{(\bar{\nu}_m + \bar{\nu}_i)} K_{\sigma_i} \right] \tag{9}$$

where K_{σ_m} is equal to 1.13 and K_{σ_i} is equal to 1.95 according to Ref. (1).

Using the data for equilibrium air composition at various temperatures and

densities, given in Ref. (4), the theoretical conductivity has been calculated and is shown in Fig. (1).

At the lower temperatures where $\bar{\nu}_m$ is the dominant collision influence, the conductivity is nearly linearly proportional to the electron number density, the temperature to the one half power dependence of $\bar{\nu}_m$ being much weaker than the nearly exponential dependence of electron number density on temperature. At the higher temperatures, where the air approaches the fully ionized state and thus the electron number density approaches a constant at $n_{e_{max.}}$, the temperature to the three halves power dependence of $\bar{\nu}_i$ is dominant. At the lower densities, this change takes place at lower temperatures because at a given temperature, the degree of ionization is inversely proportional to the density.

The disagreement between this and data given in Ref. (2) appears to be due to different information used for electron number density rather than the assumption of an average collision cross section for the neutral particles. The theoretical curve of Ref. (2) is reproduced on Fig. (1) for comparison.

B - The Effect of a Conducting Medium on the Impedance of a Coil

The technique employed for measuring the electrical conductivity of gases is based on the effect of a conducting medium on the impedance of a coil.

A theoretical investigation of the problem was first undertaken to establish the feasibility of such measurements. Furthermore, it was hoped that the theoretical results would yield information that would be helpful in determining the choice of experimental parameters such as the radius of the probe coil, the probe excitation frequency and the length of the coil.

The general case of the finite cylindrical coil in a moving conducting

medium was considered and the results are given in Appendix I.

Since it had been decided to use a direct calibration scheme, evaluation of the general case which would require a computer program was not considered necessary.

The case of the infinite coil for which the impedance is given by:

$$\frac{E}{I} = \pi^2 R^2 \mu \omega J_1(\sqrt{-iR_M})\, H_1^{(2)}(\sqrt{-iR_M}) \qquad (10)$$

was evaluated, however, in order to obtain information on the coil radius, and excitation frequency which would yield measurable results for the expected values of R_M, (R_M is the magnetic Reynolds number defined by $R_M = \sigma \mu_o \omega R^2$, where R is the radius of the coil, ω is the excitation frequency, μ_o is the permeability of free space, and σ is the electrical conductivity of the medium surrounding the coil.)

Since no information was obtained on the effect of the length of the probe coil, it was chosen as the longest length that would be completely immersed in the test gas for the range of test conditions desired and the geometry of the shock tube.

Utilizing the information obtained from the theoretical results, the probe coil radius was chosen as 4 mm. This choice was based on a compromise between probe sensitivity and fluid dynamic effects on the shock tube flow.

The excitation frequency was chosen as, $\omega = 30 \times 10^6$, (~ 5 Mc). This choice was based on the probe sensitivity and the consideration of the various frequencies which are discussed below.

The average electron collision frequency for the range of the present experiments is of the order of 10^{11} to 10^{13}, which when compared to ω, shows

that the condition $\omega << \bar{\nu}$ is satisfied.

The resonant electron excitation frequency, or plasma frequency, $\omega_{p_e} = \sqrt{n_e e^2/\pi m_e}$, which varies from 10^{11} to 10^{12} for the range of conditions investigated, may also be compared to ω to show that the condition $\omega << \omega_{p_e}$ is satisfied.

The resonant frequency ωp_{NO^+} of the heaviest ion NO^+ may also be considered although it is doubtful that with the damping due to collisions the ions could significantly effect the conductivity even at resonance. In the range investigated, the resonant frequency for NO^+ varies from 6×10^8 to 6×10^9.

Comparing the lowest value of ωp_{NO^+} to ω shows it to be of the order of 20 times ω.

The above comparisons show that the assumptions of the theory for the conductivity of the ionized gas are indeed satisfied and that phenomena associated with resonant excitation of the plasma particles should not be encountered in the present range of experiments.

II. Experimental Equipment

A - Shock Tube

The facility employed in this research was designed to be used as a tailored-interface shock tunnel. For this project, however, it is used as a closed-end shock tube. A schematic of the tube and instrumentation is shown in Fig. (3). The driver section has a six and one half inch inside diameter and is designed to withstand a pressure of 30,000 psi. For safety, the maximum operating pressure is limited to 10,000 psi.

A stoichiometric mixture of hydrogen and oxygen diluted with helium is

used as the driver gas. The driver charge is introduced through a pressure tubing leading to 4 ports in the driver section and is ignited by ordinary spark plugs. The partial pressures of the mixture are measured with high accuracy bourdon tube gages, as the various components are introduced.

Four different diaphragms were used for the tests reported. The diaphragms are scored at right angles to insure that they will burst into four petals.

1. .125" annealed copper scored .018" deep.
   Nominal breaking pressure 2200 psia.

2. .062" annealed copper scored .009" deep.
   Nominal breaking pressure 1000 psia.

3. .093" aluminum scored .009" deep.
   Nominal breaking pressure 700 psia.

4. .063" aluminum scored .007" deep.
   Nominal breaking pressure 350 psia.

The tube section has a 3 1/2" inside diameter and is designed to withstand 10,000 psi. For safety reasons the pressure was limited to 3,000 psi.

Several ports along the tube are used for shock speed and pressure measuring instrumentation.

B - Instrumentation

1. Shock Speed Measurement

Ordinary spark plugs are used to detect the ionization behind the shock wave. In the circuit used, the spark plug gap replaces the resistor normally found at the transistor base of the first stage of a two stage emitter follower amplifier. The change in gap resistance when the shock wave passes produces a sharp voltage change which is used to gate microsecond counters. Only a single wire in addition to the ground lead to each spark plug location is

required with this circuit, and the emitter follower amplifier is constructed into a small tubular unit, Fig. (16), which screws directly onto the spark plug electrode. The wiring diagram of this circuit is given in Fig. (4).

One interval of the shock speed measurement is obtained on a Hewlett Packard 523 C/R counter which has its own trigger circuit, the other two intervals are measured on a counter of special design which makes use of the trigger circuit shown in Fig. (8).

The standard 1 MC. signal output of the Hewlett Packard counter is fed into the pulse amplifier which amplifies and shapes the input signal to the requirements of the counter decades. The output signal of the pulse amplifier is then gated by the multivibrator circuits which are triggered by the emitter follower amplifiers on the ionization plugs.

2. Pressure Measurement

Pressure measurements in both the driver and tube sections have been made using SLM crystal pressure transducers and electrometer amplifiers of our design. The electrometer tubes available do not require a high plate voltage and therefore are easily incorporated into a transistor circuit. A schematic diagram of the circuit is shown in Fig. (5).

The natural frequency and damping of the crystal were measured, and a filter was designed with the inverse of the transfer function of the crystal. With this filter, rather than cutting off below the natural frequency (ringing frequency) of the transducer, it is possible to measure pressure fluctuations up to the limit of the amplifier (200 KC). The high input impedance ($\sim 10^{14}$ ohms) of the amplifier allows static calibration of the pressure transducers.

3. Conductivity Measurement

As explained in section I. B, the conductivity measurements are based on the effect of a conducting medium on the impedance of a coil immersed in it. A 5 megacycle crystal controlled oscillator was designed to supply the coil excitation.

The following refers to the schematic diagram of the measuring circuit Fig. (6).

The 5 megacycle excitation current is applied to the probe through a small series resistance and a tunable series capacitor with one end of the probe coil grounded. With the capacitor properly adjusted, so that the inductance of the probe coil and the capacitor constitute a tuned series circuit for the excitation frequency, the signal at the junction between the series resistor and capacitor should represent only the resistance of the probe coil, and the signal on the other side of the resistor should be a minimum. The signal from the top of the resistor is connected through a potentiometer with appropriate series resistance to the base of the first transistor of the measuring circuit amplifier. The signal at the top of the capacitor is connected to the emitter of the first transistor. With the potentiometer properly adjusted, zero output from this first transistor can be obtained.

In effect, this allows the real part of the coil impedance to be balanced. Changes in coil impedance will then appear as an amplitude modulated signal at the first transistor.

Two amplification stages properly filtered and each followed by emitter follower stages amplify the signal, and the resulting signal is fed into an oscilloscope for recording on polaroid film.

The coil probes are constructed with a stainless steel body which is

machined to fit 9/16" high pressure tubing fittings. The probe is secured in the end plate of the shock tube with standard high pressure fittings.

The construction of the probes is accomplished in a number of steps.

The probe coil, twenty four turns of #18 copper wire, is first wound on an epoxy resin core with one lead through the center of the coil. The coil and core are assembled into the body with the center lead connected to a BNC connector and the other lead grounded to the body. The center of the body and the outside of the coil are then potted in epoxy resin. After potting, the outside of the coil is machined to the small diameter of the body and coated with a thin layer of conducting paint. After the conducting paint is dry, an opening is made in this layer along the length of the probe so that the field of the coil cannot induce circular currents in this layer. The coil end is again covered with a layer of epoxy resin and machined to the final dimensions. A cross section of the probe is shown in Fig. (2), and a photograph showing the probe in various stages of construction is shown in Fig. (17).

III. Calibration Procedure

At first it was tried to calibrate the probes by immersing them in conducting liquid solutions. Saturated sodium chloride, and a solution of potassium hydroxide of known concentration were used at various temperatures. The capacitive effects between unshielded probes and the conducting solutions indicated that this method of calibration would not be satisfactory.

It was thought at that time, that the dielectric constant for the conducting gas could be taken as unity and that no capacitive effects between the conducting gas and the probe would be evident. Effects of the strong electric field at the end of the probe coil and the fact that the dielectric constant of the conducting gas is not

exactly unity were overlooked.

A method was then devised for simulating the conducting gas, with dielectric constant unity, by a number of cylindrical layers around the probe coil substituting a conducting coil for each layer. Values for the substituted coils were determined as follows.

If we take one such layer of finite length l, mean radius r, and thickness Δr as shown in Fig. (7), this layer will be simulated by a coil of n turns of radius r and length l.

If V is the voltage induced in the conducting layer, it must aiso be the voltage induced in the simulating coil

$$V = 2\pi rnE$$

where n is the number of turns, r the radius of the coil, and E is the electric field of the probe coil.

If j is the current density in the conducting layer, the total current in the conducting layer must equal the sum of the currents in the simulating coil.

$$nI = jl\Delta r$$

and

$$\frac{V}{I} = R = \frac{n^2 E 2\pi r}{jl\Delta r}$$

and since

$$\sigma E = j$$

$$R = \frac{n^2 2\pi r}{l\Delta r} \cdot \frac{1}{\sigma}$$

where R must be the resistance of the simulating coil. If the coils are constructed of reasonably heavy copper wire, then R is the shorting resistor for the coil

in order that it may simulate the conducting layer.

The thickness of the coils must be finite, and therefore the calibration is made by making measurements with an increasing number of coils with decreasing thickness Δr and extrapolating the results to an infinite number of coils of zero thickness. Doing this for several values of conductivity, (σ), yields a calibration of coil impedance versus conductivity.

Probes calibrated in this manner showed that the capacitive effects were also present between the probe and the conducting gas.

Therefore, the probes were redesigned with an electrostatic shield to eliminate these capacitive effects. With the redesigned probes the agreement between calibration with conducting solutions and the simulation method was excellent, and the conductivity measurements in the gas were in agreement with expected results, within the accuracy of theory and previous experiments.

An additional thought on calibration may be mentioned here. If homogenous cylinders of conducting material such as are used in carbon potentiometers could be obtained with known conductivities, these cylinders could be used for calibrating the probes without resorting to the extrapolation procedure required in the present method. This method may be investigated in the future.

IV. Experimental Data

A - Range of Measurements

Using the described apparatus and procedure, data have been obtained for air over the comparatively wide range of conductivities of 5 mhos per meter to 250 mhos per meter. This corresponds to a theoretical equilibrium temperature range of 4,000°K to 8,500°K and an absolute pressure range of 150 pounds per

square inch to 400 pounds per square inch respectively. Within the accuracy of predicting the shock tube operating conditions, the density of the gas at the time of measurement was that of the atmosphere over the entire range of temperatures and pressures.

B - Effect of Reflected Shock - Interface Interaction

The ideal relationship between driver gas and test gas for conducting such measurements in the closed-end shock tube is the condition referred to as "tailored interface". This means that the initial shock after reflecting from the end plate will pass through the interface between the driven and driver gas without reflection. This condition is achieved if the acoustic impedance ratio of the driven and driver gas has a certain value which depends on the strength of the shock wave employed for compression. If the interface is tailored, the properties of the test slug contained between the interface and the shock tube end place will remain constant, except for cooling by heat transfer to the walls, until the expansion in the driver gas arrives at the interface. Relatively long test times can be realized in this manner.

For the short tube used in these experiments, the test slug will remain undisturbed for about 100 to 200 microseconds after the reflected shock has passed through the interface, if exact "tailoring" is obtained.

If the acoustic impedance of the driver gas is lower than that required for "tailoring", the interface will reflect part of the shock wave as an expansion as it passes through. This is analogous to the case of a shock wave passing out of an open ended tube into a low pressure fluid. This results in an expansion reflected from the open end into the tube.

In the case of the shock tube, the strength of the reflected expansion will depend on the shock strength and the acoustic impedance ratio. The reflected expansion after traversing the test slug, reflecting from the end plate and again traversing the test slug will interact with the interface and will produce an additional interface reflection depending on the acoustic impedance ratio across the interface at that time. These subsequent reflections will be of greatly reduced strength, however, and are of little interest in this discussion.

If the acoustic impedance of the driver gas is greater than that required for "tailoring", the shock-interface interaction will result in a reflected shock wave. This condition is analogous to the reflection of a shock at the closed end of a tube.

Thus, the analogy for the "tailored" condition is the reflection of a shock from the end of a partially closed tube with the proper ratio of opened to closed areas so that the shocks reflected from the closed portions would be canceled by the expansions reflected from the open portions.

If an expansion is reflected from the interface, the pressure and temperature of the test slug is lowered immediately after the initial conditions are established by the initial shock wave. Similarly, a shock wave reflected from the interface will result in an increase of pressure and temperature following the initial conditions.

In the experiments reported in this paper, only data recorded during the time before effects of reflections from the interface are observed are used for evaluation of the conductivity.

As may be seen in Fig. (9) the pressure is affected only slightly by

reflections from the interface; the effect on the conductivity, however, is very pronounced. This is expected since the conductivity is nearly linearly dependent on the electron number density and the electron number density depends exponentially on the temperature in the range of the present measurements. For example, at 6,000°K a ten percent increase in temperature corresponds to an eighty percent increase in conductivity.

For this reason, a probe such as used for these measurements is much more sensitive than a pressure transducer for indicating "tailored" conditions in a "tailored" interface shock tunnel.

With the driver gas used in these experiments (a stoichiometric hydrogen-oxygen mixture diluted with eighty percent helium) "tailoring" is obtained only at a shock Mach number of slightly less than nine, or at a corresponding theoretical equilibrium temperature of approximately 5,500°K. As may be seen in the records reproduced in Fig. (10), for times larger than those required by the shock wave to reach the interface an increase in conductivity is obtained for test temperatures below 5,500°K and a decrease in conductivity is observed for test temperatures above 5,500°K.

C - Experimental Procedure

After installation of the diaphragm between the driver section and tube section, a blind plug is inserted into the probe port and the complete system is evacuated. The system is then purged with dry air which is introduced through a liquid nitrogen cold trap. The purging procedure is repeated three to four times to insure that all moisture is removed from the tube. On the last dry air purging, the probe, which is calibrated while the tube is being purged, is inserted in the

end plate of the tube and the tube is again evacuated to less than .5 mm Hg.

The test air is then introduced into the tube section at the desired initial pressure. The pressure is measured with a mercury micromanometer. Since the method by which the test air was introduced into the tube section had a noticeable effect on the conductivity data obtained, the particular procedures which have been employed are discussed together with the data.

The combustible mixture is next introduced into the driver section. The total pressure of the combustible mixture is chosen to match the particular diaphragm installed.

After checking all instrumentation the driver mixture is ignited. The following information is recorded for each test:

a. Run number, on data sheet and photographs.

b. Driver mixture, composition and pressure.

c. Type of diaphragm used.

d. Initial tube pressure.

e. Initial temperature of probe.

f. Probe calibration.

g. Polaroid photograph of scope trace showing output of conductivity instrumentation.

h. Polaroid photograph of scope trace showing output of pressure measuring instrumentation (When Used).

i. The initial shock speed over three intervals, recorded on microsecond counters.

D - Evaluation of Data

The shock speed data are plotted as shock speed versus distance along the tube and the curve is extrapolated to the end of the tube. Extrapolation errors are

minimized by having the last interval eight inches long and the last ionization pick-up three inches from the end of the tube. The value for the shock speed at the end of the tube is used to determine the equilibrium air temperature and the density using the data given in Ref. (5), the initial air temperature, and the initial tube pressure. Thus, determination of the temperatures rests on the assumption of equilibrium and the accuracy of the data in Ref. (5).

The oscilloscope recording the conductivity data is triggered by the last ionization gage which is one and one half inches upstream of the probe tip. The time required for the shock to traverse the probe and reflect from the end plate is determined from the shock speed data and the data of Ref. (5). The polaroid record is evaluated at the time when the reflected shock has left the probe tip and is traveling toward the interface. The variations in data after this time are due to reflections from the reflected shock-interface interaction.

E - Presentation of Data

The evaluated conductivity for each test is tabulated in Appendix II and is plotted on Fig. (11) against the theoretical equilibrium air temperature determined by the shock speed. For comparison, values for conductivity predicted by theory for $\rho/\rho_o = 1$ are also included in Fig. (11).

F - Discussion of Data

All measurements of electric conductivity made with probes of the final design are plotted in Fig. (11). Three different methods of introducing the test air into the tube section have been employed and the results are discussed first in relation to each of these methods.

The first method, which was used for run numbers 111 through 135 plus

run numbers 152 through 154, consisted of introducing the air into the tube through a liquid nitrogen cold trap. A valve was located between the cold trap and the tube and the air intake tubing to the cold trap was open to the atmosphere. Opening the valve allowed air to be sucked into the intake tube from the room, through the cold trap, and then through the valve into the tube.

The second method was used for runs 135 through 151. For this method, the valve was located in the intake tube of the cold trap and the tubing in the liquid nitrogen was at the evacuated pressure of the shock tube prior to the introduction of the test gas. Opening the valve allowed room air to be introduced through the cold trap into the shock tube.

The third method which has been used for all tests after run number 154 consisted of introducing the air into the tube from commercially bottled high purity air.

It may be seen by Fig. (11) that the measurements made using the first method have a considerable amount of scatter and the conductivity thus obtained is consistantly higher than in the later experiments. Runs numbered 152, 153 and 154 were accomplished by means of the first method to show that the scatter and higher conductivity measurements could be repeated and were indeed the result of the first method of introducing the gas.

A reasonable explanation for the effect of the first method on the measurement is the following: Oxygen from the atmospheric air in the cold trap coils may be liquefied and collected in the coils prior to the introduction of the test air. As the test air is introduced the temperature inside the cold trap coils is increased slightly and some of the liquefied oxygen evaporates and is carried along with the

test air. Thus an oxygen rich mixture is tested rather than pure air. Since most of the ionization at the test conditions is due to NO^+, this mixture will have a higher degree of ionization, Ref. (9), and thus a higher conductivity than pure air.

It could also be expected that the large scatter observed in the data associated with method one is the result of this increased oxygen content in the test gas, since the amount of oxygen enrichment would depend on the time between runs, the rate at which the test gas is introduced, and the quantity of test gas for a particular run.

Although there have not been a large number of tests made using the bottled air for the test gas, it appears that the scatter of the experimental results will be markedly reduced compared to the prior measurements.

It has become evident that the present shock tube arrangement should be limited to tests for which the initial shock velocity is below 3.75 M/m sec. (~ 7,000°K test temperature). The reason for this limitation being that the length of the test slug, which should be approximately 2.5" long, (calculated from the information in Ref. (5), at U_s = 3.75 M/m sec.) in actual operation may vary from 2.5" long to 1.75" long depending on the diaphragm bursting characteristics. The major loss of usable test slug length for the present tube arrangement is due to the interface not being a plane surface.

Some reasonable values have been measured for shock velocities greater than 3.75 M/m sec. but considerable scatter is observed when the test slug length is reduced by unfavorable diaphragm opening at these conditions.

The data obtained for many of the higher temperature tests have not been plotted on Fig. (11), since it was evident that the test slug was not long enough to

cover the entire probe.

An additional length of tube will be added to the present arrangement for the final measurements at the higher temperatures.

The measurements obtained are in reasonable agreement with the theoretical curve for $\rho/\rho_o = 1$. The calculated density ratio for each measurement is given in Appendix II. Although the density ratio varied by a factor of two on either side of that given for the theoretical curve in Fig. (11), it may be seen from Fig. (1) that this amount of variation in density ratio should not have a significant effect.

Comparing the reliable results with the theoretical curve shows that the measured conductivity is consistantly below the theoretical value. It should be noted that the theoretical values are based on the assumption of an average collision cross section for all the neutral particles and as was noted in I, page 5, the theoretical evaluation was primarily intended to indicate the more important characteristics of the dependence of the electrical conductivity on the temperature and density.

The value of $\overline{Q}_m = 1 \times 10^{-15}$cm. was assumed for the collision cross section of the neutral particles. If the assumed value had been $\overline{Q}_m = 1.5 \times 10^{-15}$cm., and this is not unreasonable according to Ref. (9), the agreement between the measured conductivity and the theoretical value would be remarkably close.

V. Conclusions

The measurements which have been obtained indicate that the technique described in this paper will be very useful in obtaining experimental evidence on the conductivity of high temperature, high density gases.

By increasing the length of the present shock tube there is no reason that measurements at temperatures in excess of $10,000^{\circ}K$ cannot be obtained.

In addition, the density at which the measurements are made can be increased by a factor of ten without exceeding the structural limitations of the equipment.

After the difficulties associated with introducing the test gas had been resolved, the repeatability of the measurements was within the accuracy of reading the polaroid records and the determination of the equilibrium temperature from the information in Ref. (5).

The preliminary measurements suggest that a value of $\overline{Q}_m = 1.5 \times 10^{-15}$cm. should be used for the average collision cross sections of the neutral particles if the theoretical evaluation of this paper is used to determine the electrical conductivity of air.

APPENDIX I:

The Finite Coil in a Moving Conducting Medium

We have the following basic equations due to Maxwell.

$$\nabla \times \vec{H} = \vec{j} + \epsilon \frac{\partial \vec{E}}{\partial t} \tag{1}$$

$$\nabla \times \vec{E} = -\mu \frac{\partial \vec{H}}{\partial t} \tag{2}$$

and the generalized Ohms law:

$$\vec{j} = \sigma \vec{E} + \sigma\mu (\vec{C} \times \vec{H}) \tag{3}$$

where $\vec{C}$ is the velocity of the conducting medium and all other symbols have their usual meaning as given in the List of Symbols, page (iv).

Since

$$\nabla \cdot \vec{H} = 0 \tag{4}$$

$$\oint\oint \vec{H} \cdot d\vec{s} = 0 \tag{5}$$

for the cylindrical case

$$d\vec{s} = 2\pi r(\vec{e}_x dr - \vec{e}_r dx),$$

$\vec{e}_x$ is the unit vector in x direction

$\vec{e}_r$ is the unit vector in r direction

let

$$\int\int \vec{H} \cdot d\vec{s} = \Phi(r, x, t) \tag{6}$$

and then from (2)

$$\iint (\nabla \times \vec{E}) \circ d\vec{s} = -\mu \frac{\partial}{\partial t} \iint \vec{H} \circ d\vec{s} = -\mu \frac{\partial \Phi}{\partial t} \tag{7}$$

and from (1) and (3)

$$\iint \sigma(\nabla \times \vec{E}) \circ d\vec{s} + \sigma\mu \iint \nabla \times (\vec{C} \times \vec{H}) \circ d\vec{s} + \varepsilon \frac{\partial}{\partial t} \iint (\nabla \times \vec{E}) \circ d\vec{s} = \iint \nabla \times (\nabla \times \vec{H}) \circ d\vec{s} \tag{8}$$

which reduces to

$$\sigma\mu \frac{\partial \Phi}{\partial t} - \sigma\mu \iint (\vec{C} \circ \nabla)\vec{H} \circ d\vec{s} + \mu\varepsilon \frac{\partial^2 \Phi}{\partial t^2} = -(\nabla^2 \Phi - \frac{2}{r} \frac{\partial \Phi}{\partial r}) \tag{9}$$

For a thin coil in a flow parallel to the axis of the coil for which the fluid dynamic effects on the velocity may be neglected

$$\vec{C} = \vec{e}_x U_\infty \tag{10}$$

then

$$-\sigma\mu \frac{\partial \Phi}{\partial t} - \sigma\mu U_\infty \frac{\partial \Phi}{\partial x} + \mu\varepsilon \frac{\partial^2 \Phi}{\partial t^2} = -\nabla^2 \Phi + \frac{2}{r} \frac{\partial \Phi}{\partial r} \tag{11}$$

For sinusoidal currents:

let

$$\Phi = \varphi e^{i\omega t} \tag{12}$$

then

$$-i\sigma\mu\omega\varphi + \sigma\mu U_\infty \varphi_x - \mu\varepsilon\omega^2 \varphi = -\nabla^2 \varphi + \frac{2}{r} \varphi_r \tag{13}$$

or

$$\varphi_{xx} + \varphi_{rr} - \frac{1}{r}\varphi_r + \sigma\mu U_\infty \varphi_x - \varphi(i\sigma\omega + \mu\omega^2\varepsilon) = 0 \tag{14}$$

letting

$$\varphi = r\psi \tag{15}$$

then

$$\psi_{xx} + \psi_{rr} + \frac{1}{r}\psi_r + \sigma\mu U_\infty \psi_x - \psi\left(\frac{1}{r^2} + i\sigma\mu\omega + \mu\varepsilon\omega^2\right) = 0 \tag{16}$$

let

$$\rho = \frac{r}{R} R_M^{1/2} \qquad R \text{ is the radius of the coil}$$

$$\xi = \frac{x}{\ell} R_M^{1/2} \qquad \ell \text{ is the half length of the coil}$$

where $R_M = \sigma\mu\omega R^2$.

Also denote the additional dimensionless parameters:

$$R_M' = \sigma\mu U_\infty \ell$$

$$R_M'' = \mu\varepsilon\omega^2 R^2$$

then

$$\lambda^2\psi_{\xi\xi} + \psi_{\rho\rho} + \frac{1}{\rho}\psi_\rho + \lambda^2 \frac{R_M'}{R_M^{1/2}}\psi_\xi - \psi\left(\frac{1}{\rho^2} + i + \frac{R_M''}{R_M}\right) = 0 \tag{17}$$

where $\lambda = \frac{R}{\ell}$ which may be considered as the aspect ratio of the coil.

We have from (6)

$$H_x = \frac{1}{2\pi r}\frac{\partial\Phi}{\partial r}$$

$$H_r = -\frac{1}{2\pi r}\frac{\partial\Phi}{\partial x} \tag{18}$$

The boundary conditions are for $r = R$ or $\rho = R_M^{1/2}$

$$H_x(R_M^{1/2} - 0) - H_x(R_M^{1/2} + 0) = I_o\left\{1\left[\frac{\ell(\xi + R_M^{1/2})}{R_M^{1/2}}\right] - 1\left[\frac{\ell(\xi - R_M^{1/2})}{R_M^{1/2}}\right]\right\} \tag{19}$$

$$\Phi(R_M^{1/2} - 0) - \Phi(R_M^{1/2} + 0) = 0$$

From (15) and (18)

$$H_x = \frac{1}{2\pi r}\left(\psi + r\frac{\partial \psi}{\partial r}\right) \tag{20}$$

Substituting into equation (19)

$$\frac{\partial \psi}{\partial \rho}_- - \frac{\partial \psi}{\partial \rho}_+ = \frac{2\pi R}{R_M^{1/2}} I_o \left\{ 1\left[\frac{\ell(\xi + R_M^{1/2})}{R_M^{1/2}}\right] - 1\left[\frac{\ell(\xi - R_M^{1/2})}{R_M^{1/2}}\right]\right\} \tag{21}$$

$$\psi_- = \psi_+$$

The Fourier Transform in ξ is given by:

$$\bar{\psi} = \int_{-\infty}^{\infty} \psi e^{-ip\xi} d\xi \tag{22}$$

The Fourier Transform of equation (17) is then:

$$\bar{\psi}'' + \frac{1}{\rho}\bar{\psi}' - \bar{\psi}\left[\frac{1}{\rho^2} + (\lambda^2 p^2 + \frac{R_M''}{R_M}) + i(1 - p\lambda\frac{R_M'}{R_M^{1/2}})\right] = 0 \tag{23}$$

The transformed boundary conditions (21) become

$$\bar{\psi}'_- - \bar{\psi}'_+ = \frac{2\pi R}{R_M^{1/2}} I_o \int_{-\infty}^{\infty} \left\{ 1\left[\frac{\ell(\xi + R_M^{1/2})}{R_M^{1/2}}\right] - 1\left[\frac{\ell(\xi - R_M^{1/2}}{R_M^{1/2}}\right]\right\} e^{-ip\xi} d\xi \tag{24}$$

$$\bar{\psi}'_- - \bar{\psi}'_+ = \frac{2\pi R}{R_M^{1/2}} I_o \int_{-R_M^{1/2}}^{R_M^{1/2}} e^{-ip\xi} d\xi \tag{25}$$

$$\bar{\psi}'_- - \bar{\psi}'_+ = \frac{4\pi R}{R_M^{1/2}} I_o \frac{\sin p R_M^{1/2}}{p} = 4\pi R I_o \frac{\sin v}{v} \tag{26}$$

where $v = pR_M^{1/2}$

and

$$\bar{\psi}_- = \bar{\psi}_+ \tag{27}$$

The solution to equation (23) is given by

$$\text{for } \rho \geq R_M^{1/2} \quad , \qquad \bar{\psi} = AH_1^{(2)}(\beta\rho)$$

$$\rho \leq R_M^{1/2} \quad , \qquad \bar{\psi} = BJ_1(\beta\rho)$$

where

$$\beta = \sqrt{-\left[\left(\lambda^2 p^2 + \frac{R_M''}{R_M}\right) + i\left(1 - p\lambda \frac{R_M'}{R_M^{1/2}}\right)\right]}$$

for $\rho = R_M^{1/2}$, and $\beta R_M^{1/2} = u$

$$AH_1^{(2)}(u) = BJ_1(u) \tag{28}$$

Equation (25) gives

$$A\beta H_o^{(2)}(u) - \frac{A}{R_M^{1/2}} H_1^{(2)}(u) - \beta B J_o(u) + \frac{B}{R_M^{1/2}} J_1(u) = 4\pi R I_o \frac{\sin v}{v} \tag{29}$$

then

$$A = B \frac{J_1(u)}{H_1^{(2)}(u)}$$

and

$$B\left[\frac{J_1(u)H_o^{(2)}(u)}{H_1^{(2)}(u)} - J_o(u)\right] = \frac{4\pi R I_o}{u} R_M^{1/2} \frac{\sin v}{v}$$

but

$$J_1(u)H_o^{(2)}(u) - J_o(u)H_1^{(2)}(u) = \frac{2}{i\pi u}$$

so

$$B = 2\pi^2 i R R_M^{1/2} I_o H_1^{(2)}(u)$$

then

$$\bar{\psi} = 2\pi^2 R R_M^{1/2} I_o \frac{\sin v}{v} J_1(u)H_1^{(2)}(u) \tag{30}$$

and taking the inverse transform of equation (30)

$$\psi = i\pi R R_M^{1/2} I_o \int_{-\infty}^{\infty} J_1(u)H_1^{(2)}(u) \frac{\sin v}{v} e^{ip\xi} dp \tag{31}$$

$$\psi_{ave.} = \frac{1}{2R_M^{1/2}} \int_{-R_M^{1/2}}^{R_M^{1/2}} \psi \, d\xi \tag{32}$$

$$\psi_{ave.} = \frac{i\pi R I_o}{2} \int_{-\infty}^{\infty} \int_{-R_M^{1/2}}^{+R_M^{1/2}} J_1(u)H_1^{(2)}(u) \frac{\sin v}{v} e^{ip\xi} d\xi dp \tag{33}$$

then

$$\psi_{ave.} = i\pi R I_o \int_{-\infty}^{\infty} J_1(u)H_1^{(2)}(u) \frac{\sin^2 v}{v^2} dv \tag{34}$$

where

$$v = p R_M^{1/2}$$

$$u = \beta R_M^{1/2} = \sqrt{-[(\lambda^2 v^2 + R_M'') + i(R_M - \lambda v R_M')]}$$

Special Cases

(1) Low Frequency, $R_M'' \rightarrow 0$

(2) Infinitely Long Coil, $\lambda \rightarrow 0$

(3) Stationary Conducting Medium, $R_M' \rightarrow 0$

Condition (1) may be fulfilled by choosing the excitation frequency. If condition (2) is assumed, it is not necessary to consider condition (3) since the moving medium would have no effect on an infinitely long coil, $(\vec{C} \times \vec{H}) = 0$ if the velocity is along the axis of the coil.

For (1) and (2) then

$$u = \sqrt{-iR_M}$$

which is independent of p and v for R_M constant, then:

$$\Psi_{ave.} = i\pi R I_o J_1(\sqrt{-iR_M})\, H_1^{(2)}(\sqrt{-iR_M}) \int_{-\infty}^{\infty} \frac{\sin^2 v}{v^2}\, dv \tag{35}$$

$$\Psi_{ave.} = i\pi^2 R I_o J_1(\sqrt{-iR_M})\, H_1^{(2)}(\sqrt{-iR_M}) \tag{36}$$

and

$$\Phi_{ave.} = i\pi^2 R^2 I_o J_1(\sqrt{-iR_M})\, H_1^{(2)}(\sqrt{-iR_M}) \tag{37}$$

then

$$\frac{E}{I_o} = \pi^2 R^2 \mu\omega J_1(\sqrt{-iR_M})\, H_1^{(2)}(\sqrt{-iR_M}) \tag{38}$$

which for $R_M = 0$ reduces to

$$\frac{E}{I_o} = i\pi R^2 \mu\omega \tag{39}$$

which is the impedance of an infinitely long coil in a nonconducting medium.

APPENDIX II:

Table of Data

Run No.	Diaphragm	Initial Tube Pressure mm Hg.	Shock Speed M/m sec.	ρ/ρ_o	σ mhos/meter	Equilibrium Temp. ^oK
111	.091" Alum.	15	3.42	1.01	42	6220
112	.091" Alum.	15	3.40	1.00	42	6220
113	.091" Alum.	15	3.41	1.00	42	6220
114	.091" Alum.	15	3.42	1.01	21	6220
115	.125" Cu.	12	4.83	1.10	280	8370
116	.063" Cu.	13	4.13	1.08	122	7350
117	.063" Cu.	40	2.86	2.13	18	4940
118	.091" Alum.	30	3.08	1.76	22	5460
119	.091" Alum.	30	3.03	1.72	13	5300
120	.091" Alum.	30	3.03	1.72	18	5320
121	.063" Cu.	40	3.12	2.37	53	5540
122	.063" Cu.	40	3.10	2.31	29.5	5520
123	.063" Cu.	40	3.10	2.31	35	5520
124	.063" Cu.	40	3.10	2.31	26	5500
125	.063" Cu.	40	3.22	2.42	42	5850
126	.063" Cu.	40	3.10	2.31	28	5500
127	.125" Cu.	12	4.41	1.04	144	7800
128	NO DATA					
129	.091" Alum.	5	4.37	0.455	101	7420
130	NO DATA					

Run No.	Diaphragm	Initial Tube Pressure mm Hg.	Shock Speed M/m sec.	ρ/ρ_o	σ mhos/meter	Equilibrium Temp. ^oK
131	.091" Alum.	8	4.00	0.675	43	7130
132	NO DATA					
133	.125" Cu.	10	4.41	0.910	252	7830
134	.125" Cu.	10	4.84	0.990	250	8330
135	.063" Cu.	50	3.03	2.83	27	5350
136	.063" Alum.	50	2.47	2.23	6	4040
137	.063" Alum.	30	2.65	1.13	6	4330
138	.063" Alum.	20	2.90	1.10	8	4930
139	.063" Cu.	18	3.58	1.48	48	6630
140	.063" Cu.	15	3.77	1.14	48	6880
141	.063" Cu.	10	3.95	0.815	55	7110
142	.125" Cu.	10	4.70	0.924	91	8160
143	.063" Cu.	15	3.76	1.13	45	6850
144	NO DATA					
145	.063" Cu.	15	3.65	1.09	44	6700
146	NO DATA					
147	.063" Cu.	5	4.48	0.463	98	7500
148	.063" Cu.	5	4.63	0.474	44	7630
149	NO DATA					
150	.091" Alum.	20	3.12	1.18	15	5490
151	.091" Alum.	20	3.22	1.21	14	5720
152	.063" Cu.	15	3.70	1.10	56	6800

Run No.	Diaphragm	Initial Tube Pressure mm Hg.	Shock Speed M/m sec.	ρ/ρ_o	σ mhos/meter	Equilibrium Temp. ^oK
153	.063" Cu.	40	3.12	2.37	35	5530
154	.063" Cu.	40	3.06	2.25	29	5350
155	.063" Cu.	40	3.10	2.31	15	5450
156	NO DATA					
157	.063" Cu.	20	3.75	1.49	52	6900
158	.063" Alum.	20	3.10	1.20	8.5	5400
159	.063" Alum.	25	2.87	1.35	5	4810
160	NO DATA					
161	.063" Alum.	15	3.30	0.968	21.5	5870

LIST OF REFERENCES

1. Ginzburg, V. L.
   Gurevich, A. V.
   "Nonlinear Phenomena in a Plasma Located in an Alternating Electromagnetic Field", Usp. Fiz. Nauk 70, pp. 201-246, February 1960.

2. Lin, S. C.
   "Electrical Conductivity of Thermally Ionized Air Produced in a Shock Tube", AVCO Res. Note 26, February 1957.

3. Savic, P.
   Bolt, G. T.
   "A Frequency Modulation Circuit for the Measurement of Gas Conductivity and Boundary Layer Thickness in a Shock Tube", Mech. Eng. Rept. No. MT-32, National Research Council of Canada, May 1961.

4. Hilsinrath, J.
   Klein, M.
   Woolley, H.
   "Tables of Thermodynamic Properties of Air Including Dissociation and Ionization from 1500°K to 15000°K", AEDC-TR-59-20, Thermodynamic Section, National Bureau of Standards, December 1959.

5. Feldman, S.
   "Hypersonic Gas Dynamic Charts for Equilibrium Air", AVCO Research Laboratory, January 1957.

6. Manheimer-Timnat, Y.
   Low, W.
   "Electron Density and Ionization Rate in Thermally Ionized Gases Produced by Medium Strength Shock Waves", Journal of Fluid Mechanics, Vol. 6, Part 3, pp. 449-461, October 1959.

7. Margenau, H.
   "Conduction and Dispersion of Ionized Gases at High Frequencies", Phy. Rev. 69, 2nd Series, pp. 508-513, 1946.

8. Spitzer, L.
   Harm, R.
   "Transport Phenomena in a Completely Ionized Gas", Phy. Rev. 89, 2nd Series, pp. 977-981, 1953.

9. Lin, S. C.
   "Ionization Phenomenon of Shock Waves in Oxygen-Nitrogen Mixtures", AVCO Res. Rept. 33, June 1958.

10. Jahnke, E.
Emde, F.
"Tables of Functions", 4th Edition, Dover Publications.

11. Lin. S. C.
"A Rough Estimate of the Attenuation of Telemetering Signals Through the Ionized Gas Envelope Around a Typical Re-entry Missile", AVCO Res. Rept. 74, February 1956.

12. Lin, S. C.
Neal, R. A.
Fyfe, W. I.
"Rate of Ionization Behind Shock Waves in Air" I. Experimental Results, AVCO Res. Rept. 105, September 1960.

FIG. 1 LOW FREQUENCY CONDUCTIVITY OF AIR VS TEMPERATURE FOR VARIOUS DENSITIES

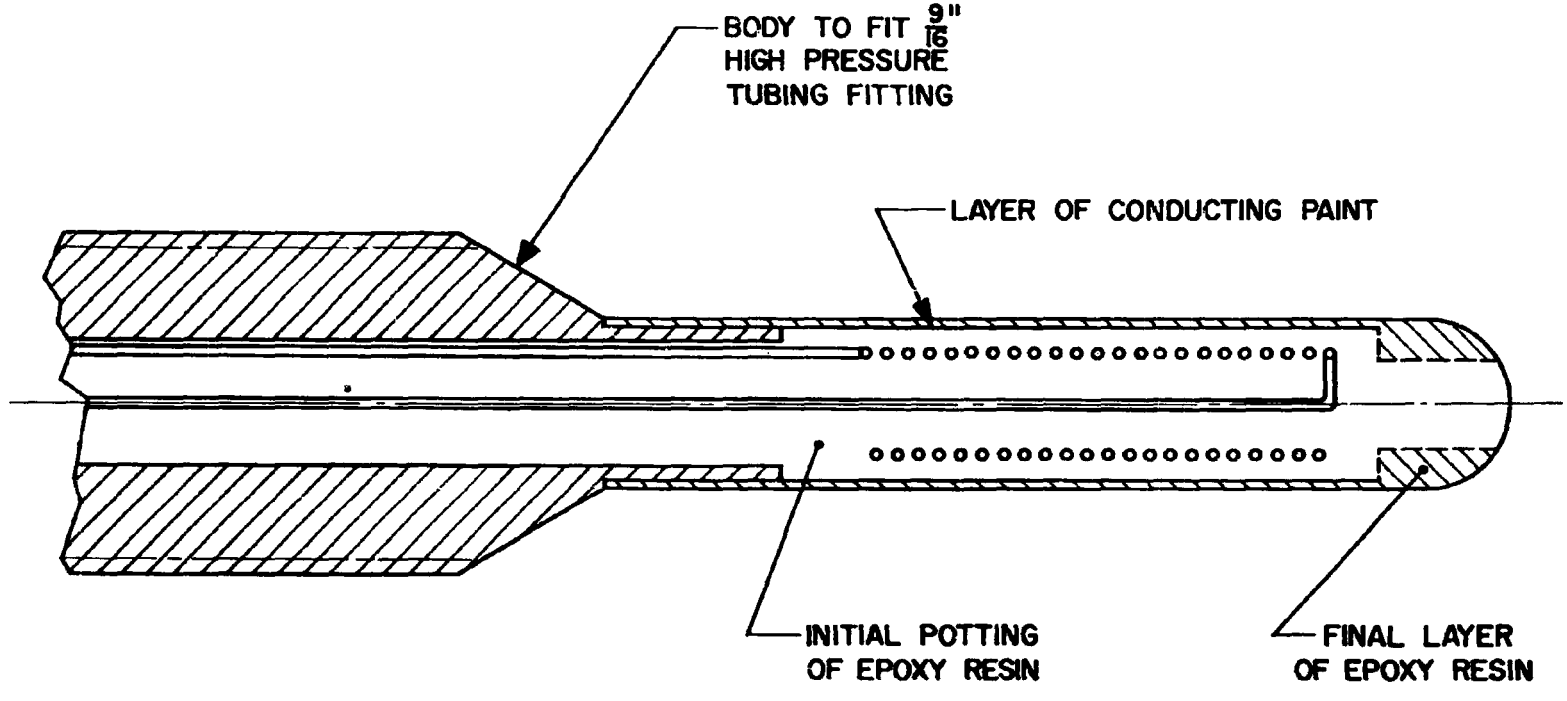

FIG. 2 PROBE CROSS SECTION

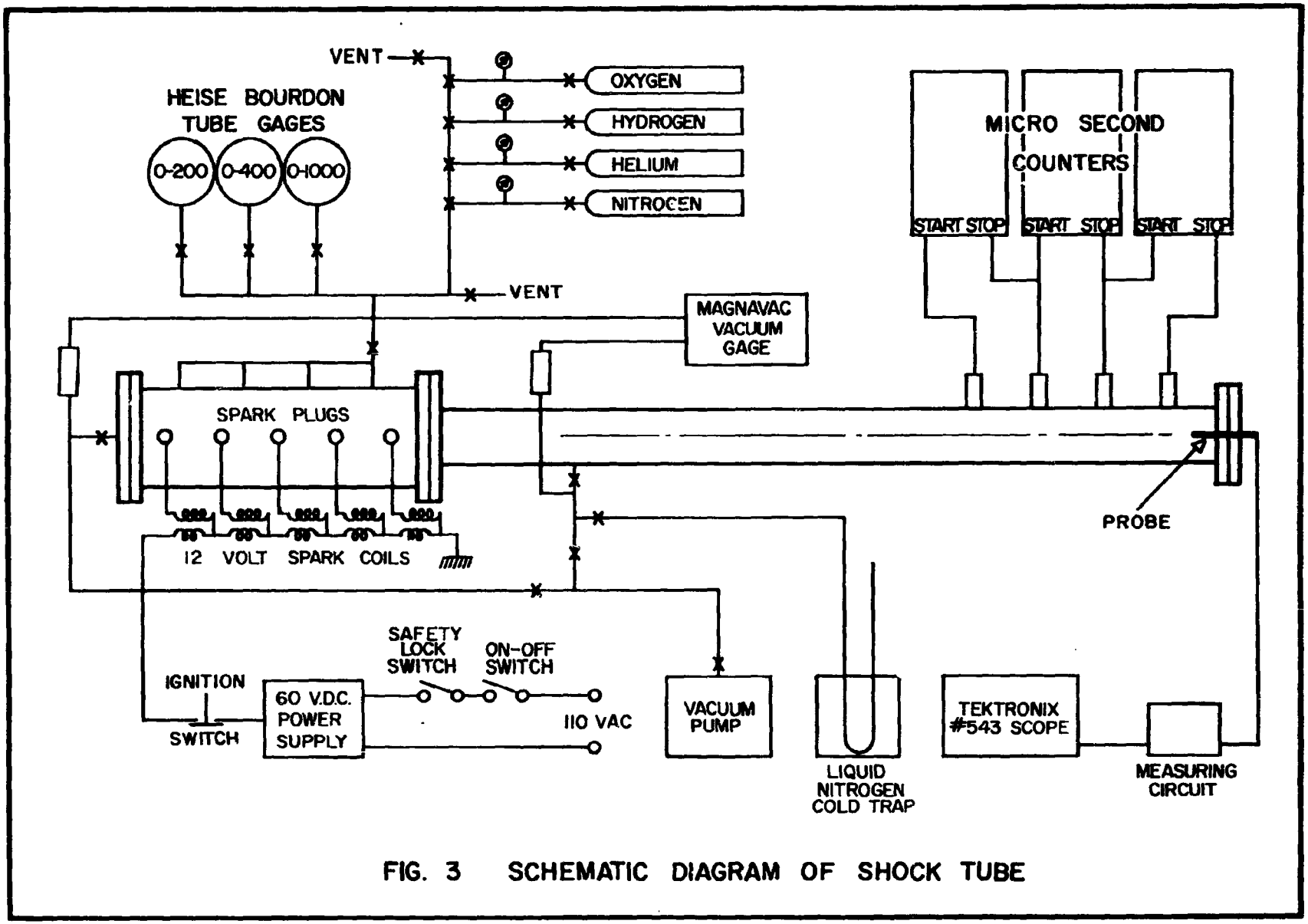

FIG. 3 SCHEMATIC DIAGRAM OF SHOCK TUBE

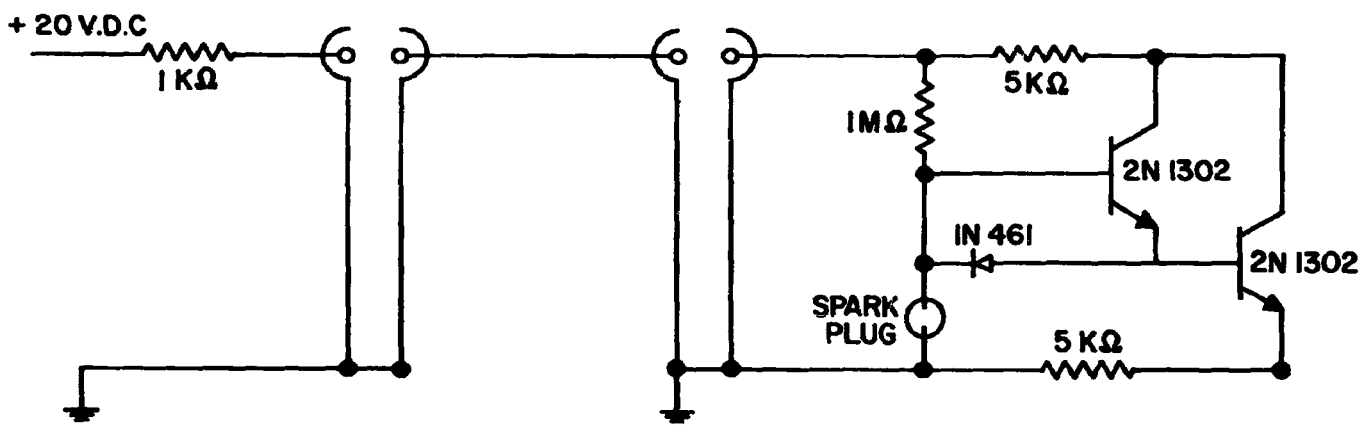

FIG. 4 EMITTER FOLLOWER AMPLIFIER

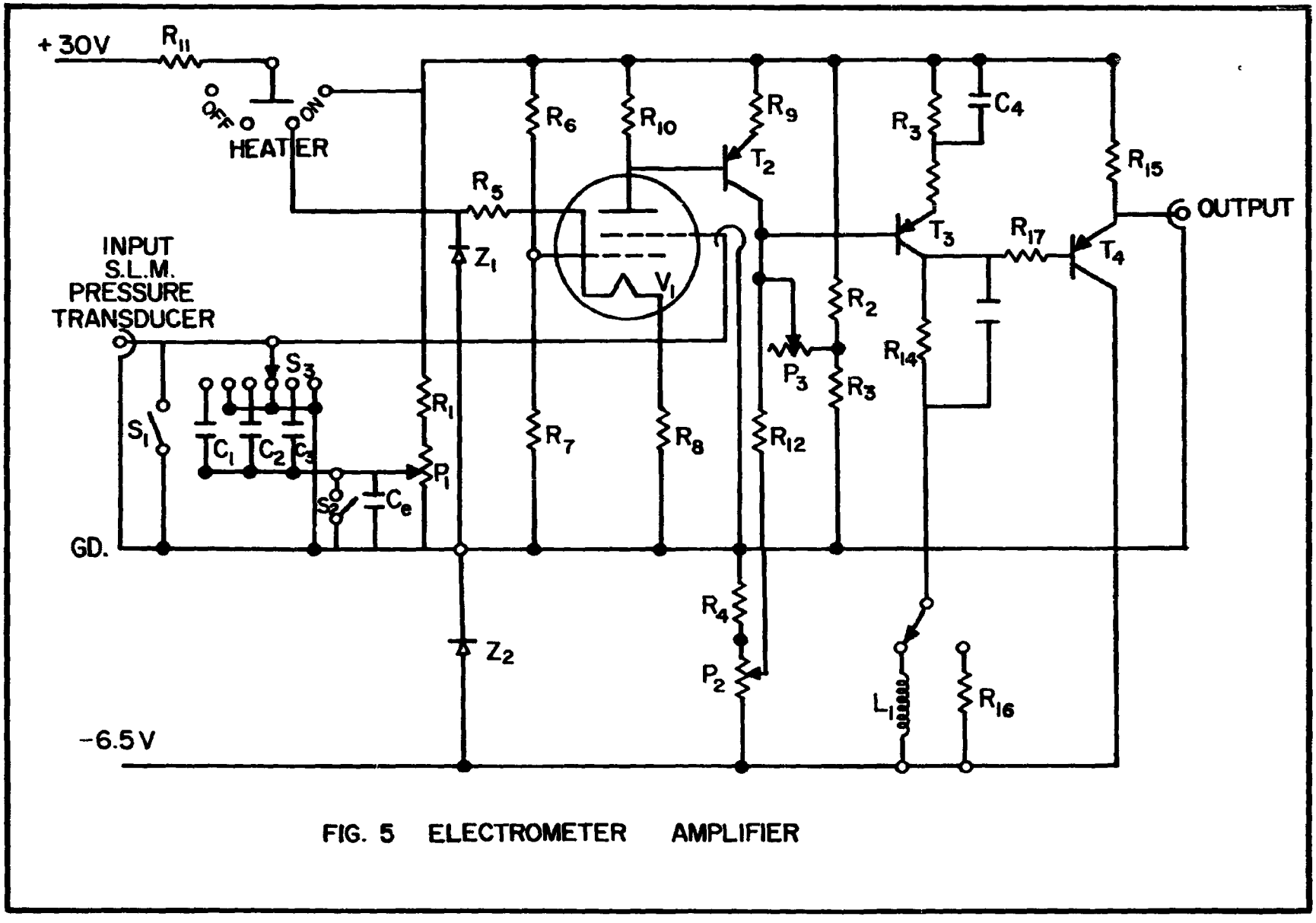

FIG. 5 ELECTROMETER AMPLIFIER

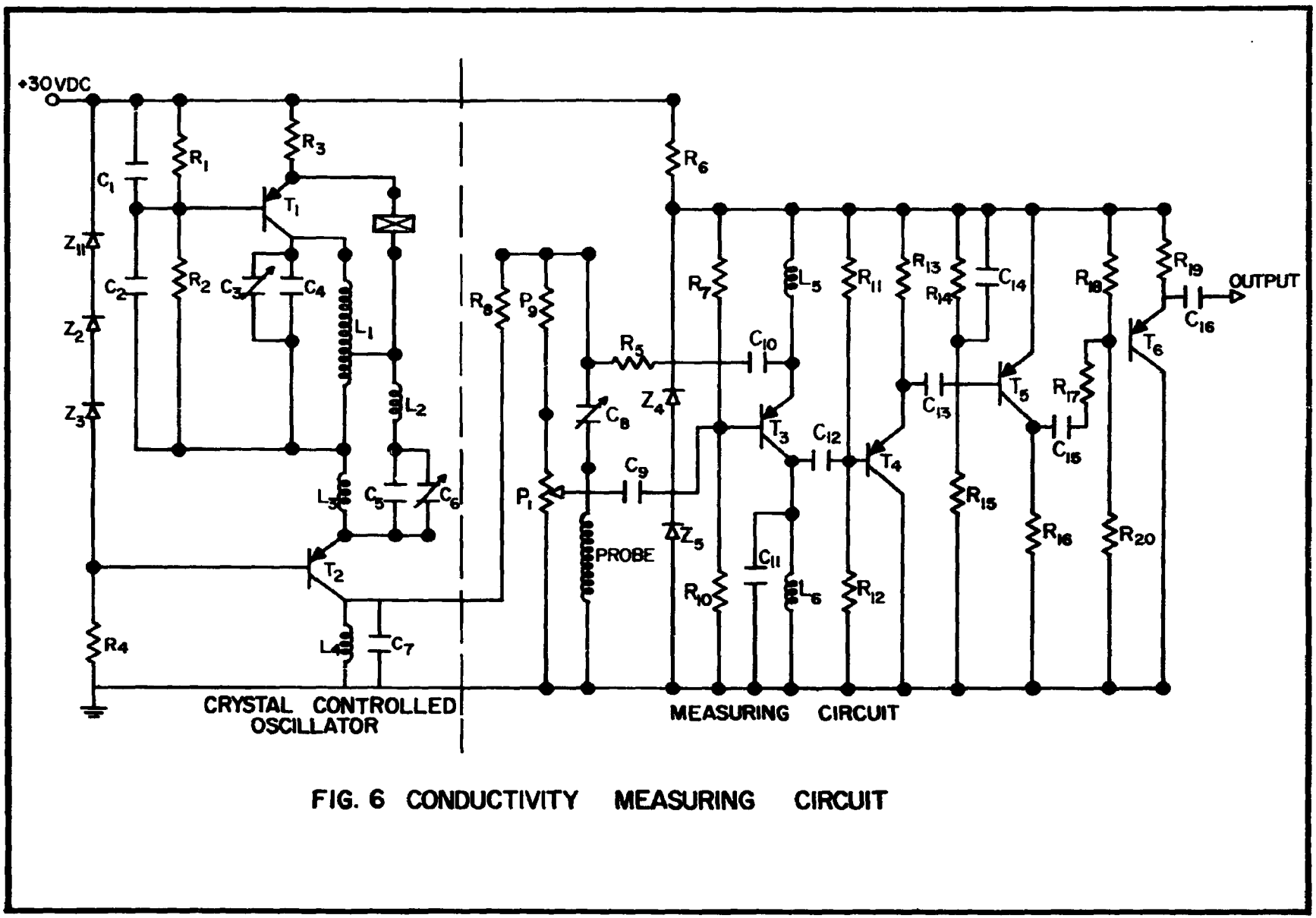

FIG. 6 CONDUCTIVITY MEASURING CIRCUIT

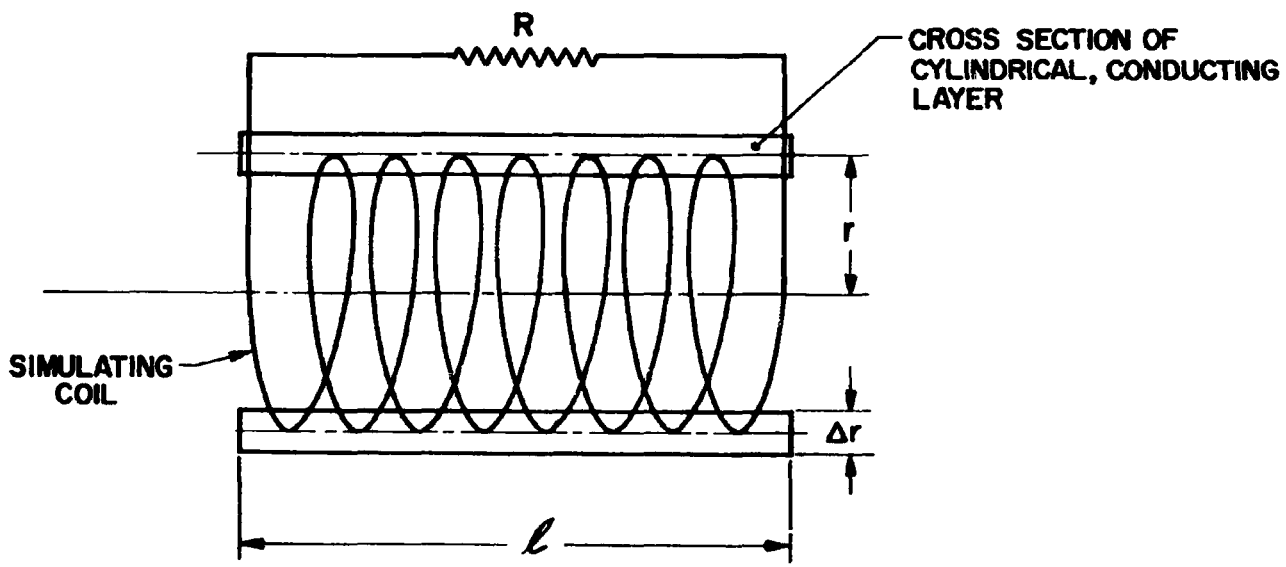

FIG. 7 CALIBRATION COIL

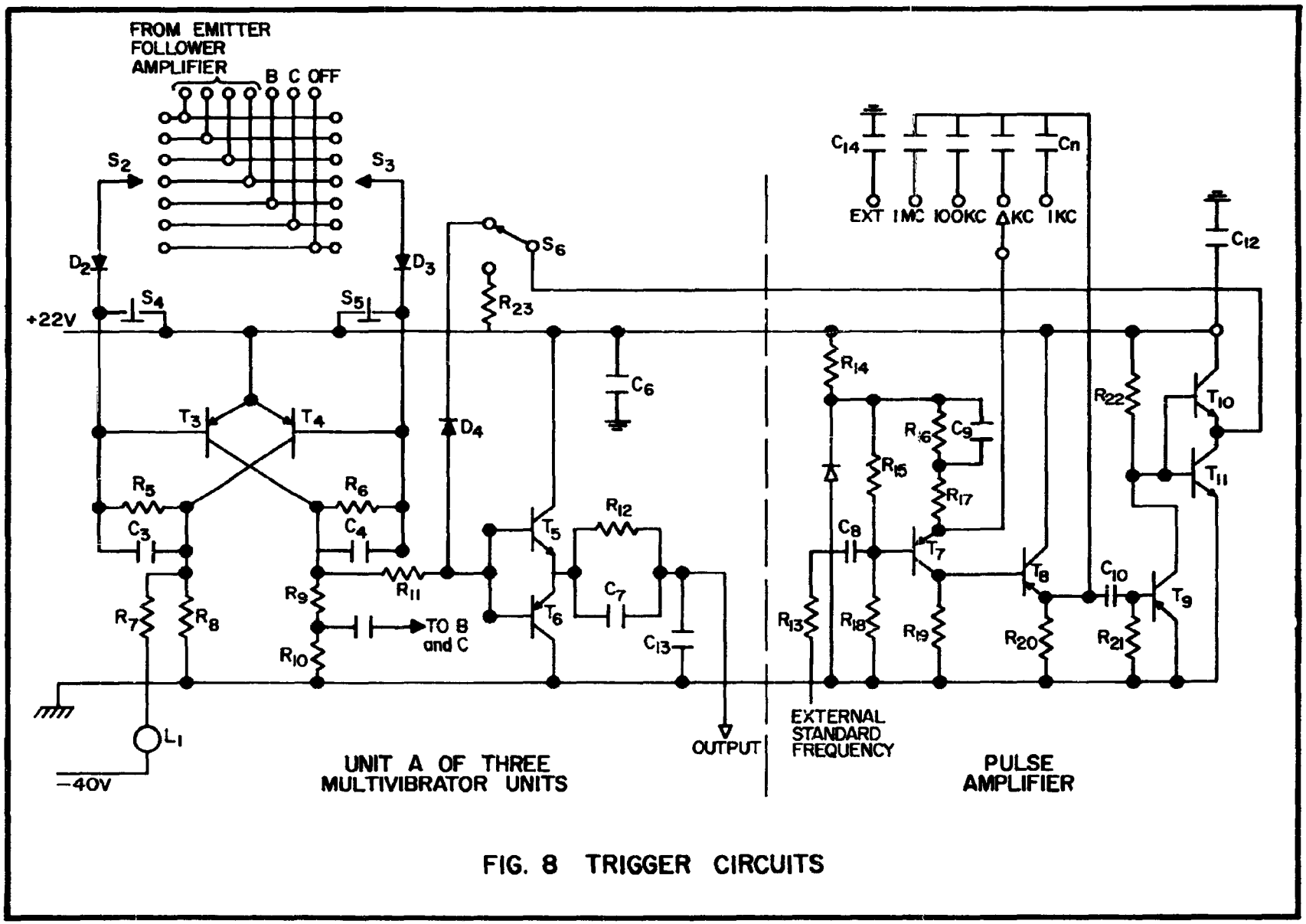

FIG. 8 TRIGGER CIRCUITS

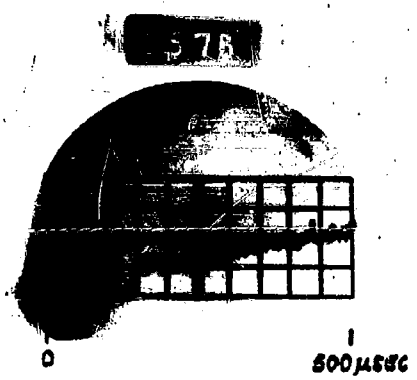

1. Pressure Record

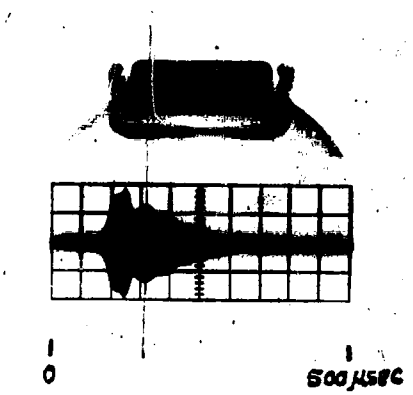

2. Conductivity Record

Fig. 9 Pressure and Conductivity Records
For Run No. 157. Us = 3.75 M/m sec., Te = 6900°K

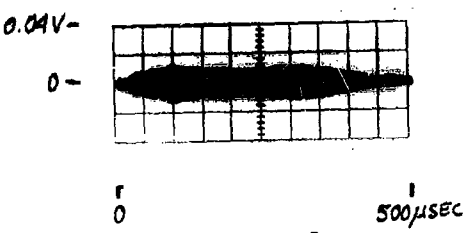

Run 138

Te = 4930°K

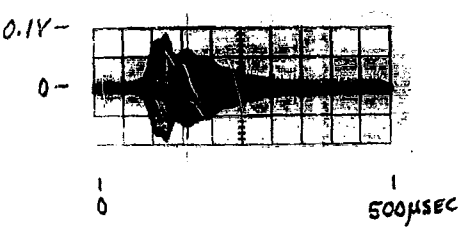

Run 157

Te = 6900°K

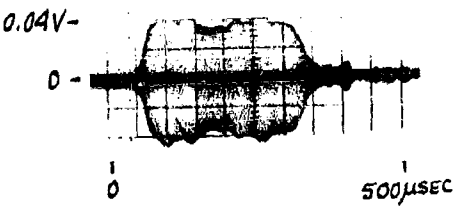

Run 118

Te = 5460°K

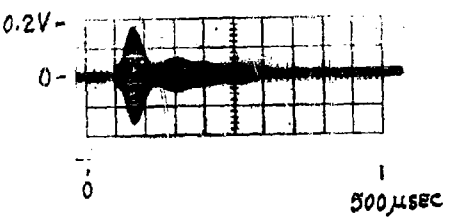

Run 116

Te = 7350°K

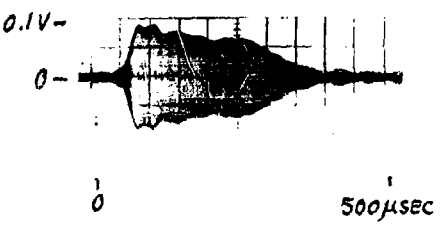

Run 121

Te = 5540°K

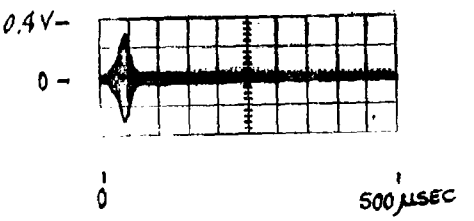

Run 133

Te = 7830°K

Fig. 10 Conductivity Records Showing the Effect of Interface Reflections

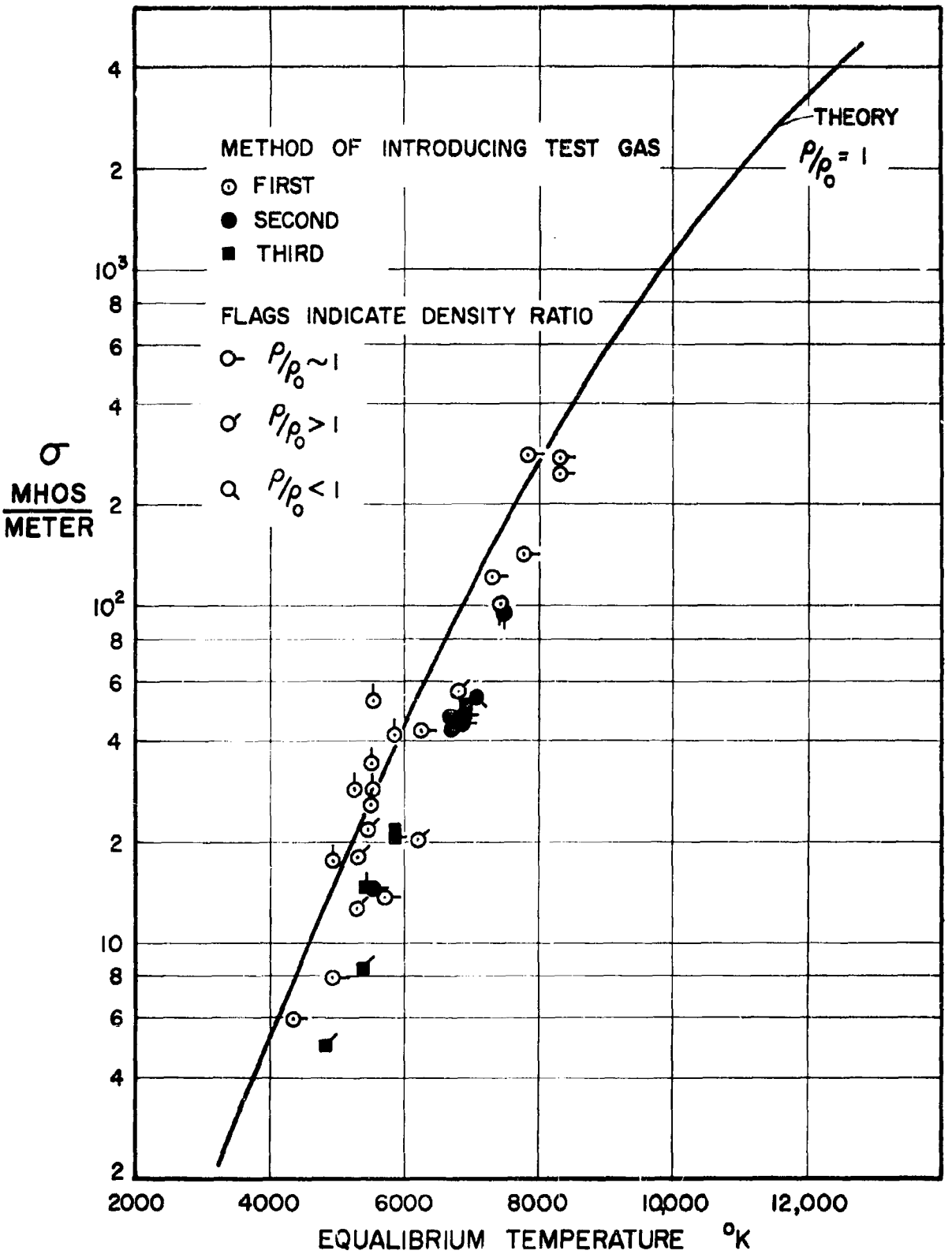

FIG. 11 EXPERIMENTAL MEASUREMENT OF ELECTRICAL CONDUCTIVITY FOR AIR

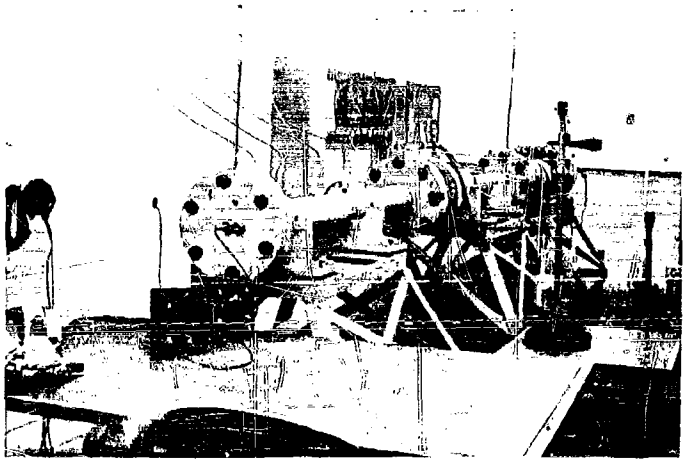

Fig. 12 The Shock Tube

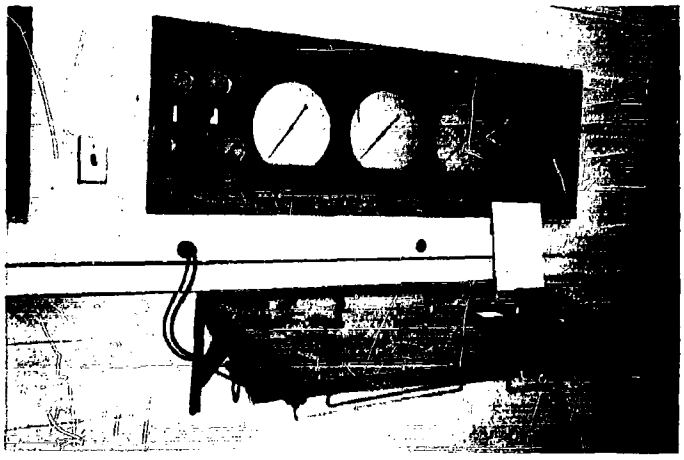

Fig. 13 Driver Gas Loading Panel

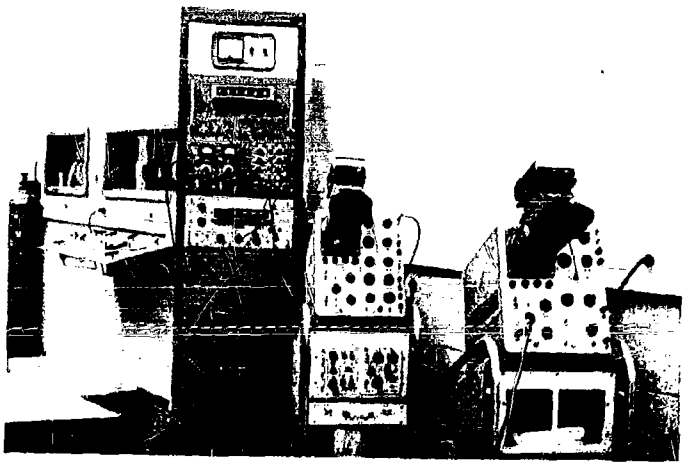

Fig. 14 Shock Tube Instrumentation

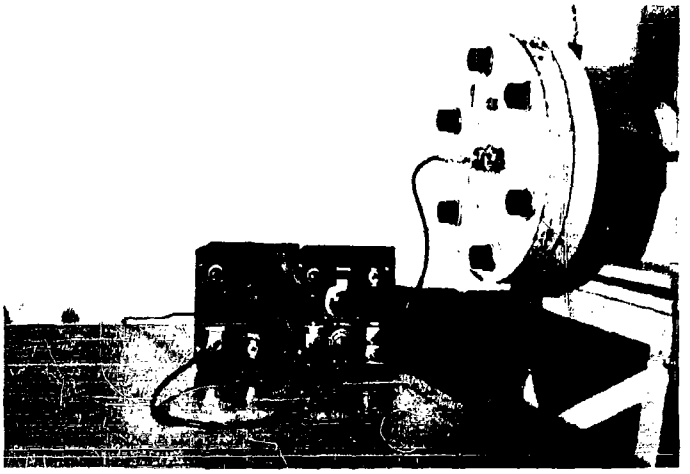

Fig. 15 Conductivity Measurement Instrumentation

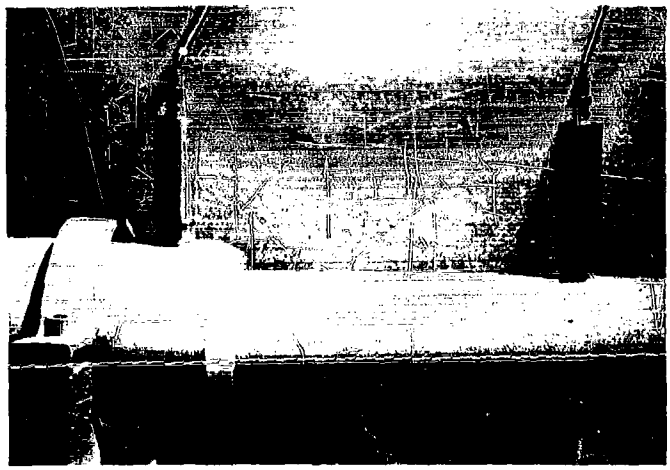

Fig. 16 Ionization Gage and Emitter Follower Amplifier

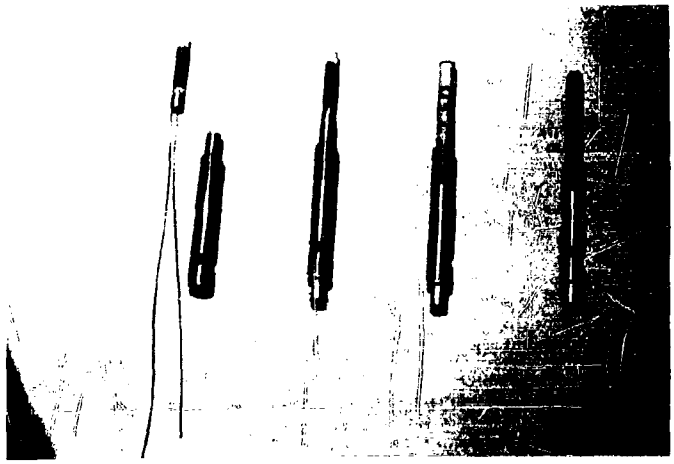

Fig. 17 Probes in Various Stages of Fabrication

(ONE COPY UNLESS OTHERWISE NOTED)

DISTRIBUTION LIST
AIR FORCE OFFICE OF SCIENTIFIC RESEARCH

18 SEPTEMBER 1959

This supercedes all previous distribution lists.

AIR FORCE

Commander — 10 copies
Armed Services Technical Information Agency
ATTN: TIPDR
Arlington Hall Station
Arlington 12, Virginia

Commander
Air Force Ballistic Missile Division
ATTN: WDSOT
Air Force Unit Post Office
Los Angeles 45, California

Commander — 4 copies
Air Force Office of Scientific Research
ATTN: Mechanics Division (2)
Library, SRLT (2)
Tempo X
Washington 25, D. C.

Commander, European Office — 2 copies
Air Research and Development Command
Shell Building
47 rue Cantersteen
Brussels, Belgium

Commander
Air Materiel Command
Wright-Patterson Air Force Base
ATTN: Library
Ohio

Commander
Air Research and Development Command
ATTN: Library
Andrews Air Force Base
Washington 25, D. C.

Commander
Arnold Engineering Development Center
ATTN: AEOI
Post Office Box 162
Tullahoma, Tennessee

Commander
Air Force Flight Test Center
ATTN: FTOTL
Edwards Air Force Base
Muroc, California

Commander
Air Force Special Weapons Center
ATTN: SWOI
Kirtland Air Force Base
New Mexico

Commander Air Force Missile Development Center
ATTN: HDOI
Holloman Air Force Base
Alamogordo, New Mexico

Commander
Air Force Missile Test Center
ATTN: MTOI
Patrick Air Force Base
Cocoa, Florida

Commander — 8 copies
Wright Air Development Center
ATTN: Aircraft Laboratory (1), WCOSI (2), WCOSR (2)
Aeronautical Research Laboratory (1), WCLC (1)
Director of Weapons Systems Operations (1)
Wright-Patterson Air Force Base, Ohio

Commandant
Air Force Institute of Technology
ATTN: MCLI
Wright-Patterson Air Force Base, Ohio

Director
Air University Library
Maxwell Air Force Base, Alabama

Commander
Air Proving Ground Center
ATTN: ACOT
Eglin Air Force Base, Florida

Commander
Air Force Cambridge Research Center
ATTN: CROT
L. G. Hanscom Field
Bedford, Massachusetts

P. O. Box AA
Wright-Patterson Air Force Base
Ohio

ARMY

Director
Ballistics Research Laboratory
ATTN: Library
Aberdeen Proving Ground, Maryland

Commanding General
Office of Ordnance Research
Department of the Army
Box CM
Duke Station
Durham, North Carolina

Commanding General
Army Rocket and Guided Missile Agency
ATTN: Technical Library, ORDXR-OOL
Redstone Arsenal, Alabama

NAVY

Chief, Office of Naval Research — 2 copies
Department of the Navy
ATTN: Mechanics Branch (1), Air Branch (1)
Washington 25, D. C.

Commanding Officer
Naval Research Laboratory
ATTN: Documents Library
Washington 25, D. C.

Commander
U. S. Naval Ordnance Library
ATTN: Library (Please route to Dr. H. H. Kurzweg)
White Oak
Silver Spring, Maryland

Commanding Officer and Director
David Taylor Model Basin
Aerodynamics Laboratory
ATTN: Library
Washington 7, D. C.

Chief, Bureau of Ordnance
Department of the Navy
ATTN: Mr. Jerome Persh, Special Projects Office, SP-2722
Washington 25, D. C.

NASA

Director
National Aeronautics and Space Administration
ATTN: Chief, Document Library
1520 H Street, N. W.
Washington 25, D. C.

5 copies

DEPARTMENT OF COMMERCE

Director
National Bureau of Standards
U. S. Department of Commerce
ATTN: Library
Washington 25, D. C.

Director
Office of Technical Services
U. S. Department of Commerce
ATTN: Technical Reports Section
Washington 25, D. C.

AGENCIES

National Science Foundation
ATTN: Engineering Sciences Division
1951 Constitution Avenue, N. W.
Washington 25, D. C.

U. S. Atomic Energy Commission
Technical Information Service
1901 Constitution Avenue, N. W.
Washington 25, D. C.

U. S. Atomic Energy Commission
Technical Information Extension
Post Office Box 62
Oak Ridge, Tennessee

JOURNALS

Southwest Research Institute
ATTN: Applied Mechanics Reviews
8500 Culebra Road
San Antonio 6, Texas

2 copies

Aeronautical Engineering Review
2 East 64th Street
New York 21, New York

Institute of Aeronautical Sciences
ATTN: Library
2 East 64th Street
New York 21, New York

EDUCATIONAL INSTITUTIONS

Brown University
Division of Engineering
ATTN: Library
Providence 12, Rhode Island

University of California
Institute of Engineering Research
Low Pressures Research Project
Berkeley 4, California

University of California
Engineering Department
ATTN: Library (Please route to Prof. M. K. Boeltes)
Los Angeles, California

Jet Propulsion Laboratory
California Institute of Technology
ATTN: Library (Please route to Dr. P. Wegener)
4800 Oak Grove Drive
Pasadena 3, California

Guggenheim Aeronautical Laboratory
California Institute of Technology
ATTN: Aeronautics Library (Please route to Professor H. W. Liepmann)
Pasadena 4, California

Carnegie Institute of Technology
ATTN: Library
Pittsburgh 18, Pennsylvania

Catholic University of America
Aeronautical Mechanical Engineering
ATTN: Library

Cornell University
Graduate School of Aeronautical Engineering
ATTN: Library (Please route to Dr. W. R. Sears)
Ithaca, New York

Columbia University
Department of Civil Engineering and Engineering Mechanics
ATTN: Library (Please route to Prof. G. Herrmann)
New York 27, New York

University of Florida
Engineering Mechanics Department
ATTN: Library
Gainesville, Florida

Georgia Institute of Technology
Department of Mechanical Engineering
ATTN: Library
Atlanta, Georgia

Harvard University
Department of Engineering Sciences
ATTN: Library
Cambridge 38, Massachusetts

Harvard University
Department of Applied Physics
ATTN: Library (Please route to Prof. H. W. Emmons)
Cambridge 38, Massachusetts

Illinois Institute of Technology
Armour Research Foundation
ATTN: Library
Chicago, Illinois

University of Illinois
Aeronautical Institute
ATTN: Library (Please route to Prof. H. O. Barthel)
Urbana, Illinois

John Crerar Library
86 E. Randolph Street
Chicago 1, Illinois

Johns Hopkins University
Applied Physics Laboratory
ATTN: Library
8621 Georgia Avenue
Silver Spring, Maryland

Johns Hopkins University
Department of Aeronautics
ATTN: Library (Please route to Dr. Francis H. Clauser)
Baltimore 18, Maryland

Lehigh University
Department of Physics
ATTN: Library (Please route to Prof. H. J. Emrich)
Bethlehem, Pennsylvania

University of Maryland
Institute for Fluid Dynamics and Applied Mathematics
College Park, Maryland

University of Maryland
ATTN: Engineering Library
College Park, Maryland

Massachusetts Institute of Technology
Naval Supersonic Laboratory
Cambridge 39, Massachusetts

Massachusetts Institute of Technology
ATTN: Library (Please route to Mech. & Aero. Engr. and Mechanics)
Cambridge 39, Massachusetts

Massachusetts Institute of Technology
Fluid Dynamics Research Group
ATTN: Dr. Leon Trilling
Cambridge 39, Massachusetts

University of Michigan
Department of Aeronautical Engineering
ATTN: Library
East Engineering Building
Ann Arbor, Michigan

Midwest Research Institute
ATTN: Library
425 Volker Boulevard
Kansas City 10, Missouri

University of Minnesota
Institute of Technology
ATTN: Engineering Library
Minneapolis, Minnesota

Rosemount Aeronautical Laboratories
University of Minnesota
Department of Aeronautical Engineering
ATTN: Library
Minneapolis, Minnesota

North Carolina State College
Division of Engineering Research
ATTN: Technical Library
Raleigh, North Carolina

Ohio State University
Department of Aeronautical Engineering
ATTN: Library
Columbus, Ohio

Polytechnic Institute of Brooklyn
Department of Aeronautical Engineering and Applied Mechanics
ATTN: Library
333 Jay Street
Brooklyn 1, New York

Aerodynamics Laboratory
Polytechnic Institute of Brooklyn
527 Atlantic Avenue
Freeport, New York

Pennsylvania State University
Department of Aeronautical Engineering
ATTN: Library
University Park, Pennsylvania

The James Forrestal Research Center
Princeton University
ATTN: Library (Please route to Prof. S. Bogdonoff)
Princeton, New Jersey

Princeton University
Department of Aeronautical Engineering
ATTN: Library
Princeton, New Jersey

Rensselaer Polytechnic Institute
Department of Aeronautical Engineering
ATTN: Library
Troy, New York

University of Southern California
Engineering Center
ATTN: Library
3518 University Avenue
Los Angeles 7, California

Stanford Research Institute
Documents Center
ATTN: Acquisitions
Menlo Park, California

Stanford University
Department of Aeronautical Engineering
ATTN: Library
Stanford, California

Defense Research Laboratory
University of Texas
Post Office Box 8029
Austin 12, Texas

University of Virginia
Ordnance Research Laboratory
Charlottsville, Virginia

University of Washington
Department of Aeronautical Engineering
ATTN: Library
Seattle, Washington

New York University
Institute of Mathematical Sciences
ATTN: Library
New York 3, New York

INDUSTRIAL ORGANIZATIONS

Allied Research Associates
ATTN: Library (Please route to Dr. T. R. Goodman)
43 Leon Street
Boston 5, Massachusetts

AVCO Manufacturing Company
Research Laboratories
ATTN: Chief, Technical Library
2385 Revere Beach Parkway
Everett 49, Massachusetts

AVCO Manufacturing Company
Research and Advanced Development Division
ATTN: Research Library, Mrs. H. M. Page
201 Lowell Street
Wilmington, Massachusetts

Bell Aircraft Corporation
ATTN: Library
Post Office Box 1
Buffalo 5, New York

Boeing Airplane Company
ATTN: Library
Post Office Box 3107
Seattle 14, Washington

Chance-Vought Aircraft, Inc.
ATTN: Library
Dallas, Texas

CONVAIR
Fort Worth Division
ATTN: Library
Fort Worth 1, Texas

CONVAIR
ATTN: Library
Post Office Box 1011
Pomona, California

CONVAIR 2 copies
Scientific Research Laboratory
ATTN: Library (Please route 1 copy to Chief, Applied Research)
Post Office Box 950
San Diego 12, California

Cornell Aeronautical Laboratories, Inc.
ATTN: Library
4455 Genesee Street
Buffalo 21, New York

Douglas Aircraft Company, Inc.
ATTN: Library
827 Lapham Street
El Segundo, California

Douglas Aircraft Company, Inc.
ATTN: Library
3000 Ocean Park Boulevard
Santa Monica, California

Fairchild Engine and Aircraft Company
Guided Missiles Division
ATTN: Library
Wyandanch, L. I., New York

Flight Sciences Laboratory
ATTN: Library
1965 Sheridan Avenue
Buffalo 23, New York

General Applied Science Laboratories, Inc.
Meadowbrook National Bank Building
60 Hempstead Avenue
Hempstead, New York

General Electric Company
Aircraft Gas Turbine Division
ATTN: Library
Cincinnati 15, Ohio

General Electric Company
Aeroscience Laboratory - MSVD
ATTN: Library (Please route to Dr. H. Lew)
3750 "D" Street
Philadelphia 24, Pennsylvania

General Electric Company
Research Laboratory
Post Office Box 1088
Schenectady 5, New York

General Electric Company
Special Defense Products Division
3198 Chestnut Street
Philadelphia 4, Pennsylvania

Grumman Aircraft Engineering Corporation
ATTN: Library
Bethpage, L. I., New York

Hughes Aircraft Company
Research and Development Laboratories
ATTN: Library
Culver City, California

Lockheed Aircraft Corporation
ATTN: Library
Post Office Box 551
Burbank, California

Lockheed Aircraft Missile Systems Division
ATTN: Library
Palo Alto, California

The Martin Company
ATTN: Library
Baltimore 3, Maryland

McDonnell Aircraft Corporation
ATTN: Library
Post Office Box 516
St. Louis 66, Missouri

North American Aviation, Inc.
Missile Division
ATTN: Library
12214 Lakewood Boulevard
Downey, California

Northrop Aircraft, Inc.
ATTN: Library
Hawthorne, California

Plasmadyne Corporation
ATTN: Library
3839 South Main Street
Santa Ana, California

The Ramo-Wooldridge Corporation
ATTN: Chief Librarian
5730 Arbor Vitae
Los Angeles 45, California

Rand Corporation
1700 Main Street
Santa Monica, California

Republic Aviation Corporation
ATTN: Library
Farmingdale, L. I., New York

RIAS Inc.
ATTN: Library
7212 Bellona Avenue
Baltimore 12, Maryland

United Aircraft Corporation
Research Department
ATTN: Library
400 Main Street
East Hartford 8, Connecticut

VITRO Laboratories
West Orange Laboratory
200 Pleasant Valley Way
West Orange, New Jersey

Westinghouse Electric Corporation
Aviation Gas Turbine Division
ATTN: Engineering Library
P. O. Box 288
Kansas City, Missouri

FOREIGN ORGANIZATIONS

Director
National Aeronautical Establishment
Ottawa, Ontario
Canada

University of Toronto
Institute of Aerophysics
ATTN: Library
Toronto 5, Canada

Trailing Center for Experimental Aerodynamics
ATTN: Library
Rhode-Saint-Genese (Belgique)
72, Chaussee de Waterloo
Belgium

Chairman
Defence Research Board
ATTN: DSIS
Ottawa, Ontario
Canada